Available online at www.sciencedirect.com
ScienceDirect
Journal of Sound and Vibration 323 (2009) 67–92
JOURNAL OF SOUND AND VIBRATION
www.elsevier.com/locate/jsvi

A method of transmissibility design for dual-chamber pneumatic vibration isolator

Jeung-Hoon Lee[a], Kwang-Joon Kim[b,*]

[a]*Propulsor Research Part, Samsung Ship Model Basin (SSMB), Marine Research Institute, Samsung Heavy Industries, Science Town, Daejeon 305-380, South Korea*

[b]*Center for Noise and Vibration Control, Department of Mechanical Engineering, Korea Advanced Institute of Science and Technology, Science Town, Daejeon 305-701, South Korea*

Received 25 March 2008; received in revised form 20 December 2008; accepted 27 December 2008
Handling Editor: L.G. Tham
Available online 6 February 2009

Abstract

Dual-chamber pneumatic vibration isolators have a wide range of applications for vibration isolation of vibration-sensitive equipment. Recent advances in precision machine tools and instruments such as medical devices and those related to nano-technology require better isolation performance, which can be efficiently achieved by precise modeling- and design- of the isolation system. This paper discusses an efficient transmissibility design method of a pneumatic vibration isolator wherein a complex stiffness model of a dual-chamber pneumatic spring developed in our previous study is employed.

Three design parameters, the volume ratio between the two pneumatic chambers, the geometry of the capillary tube connecting the two pneumatic chambers, and, finally, the stiffness of the diaphragm employed for prevention of air leakage, were found to be important factors in transmissibility design. Based on a design technique that maximizes damping of the dual-chamber pneumatic spring, trade-offs among the resonance frequency of transmissibility, peak transmissibility, and transmissibility in high frequency range were found, which were not ever stated in previous researches. Furthermore, this paper discusses the negative role of the diaphragm in transmissibility design. The design method proposed in this paper is illustrated through experimental measurements.

1. Introduction

Environmental vibrations from the ground, people's movement, and equipment operation are becoming important issues in the areas of precision engineering including nano-scale manufacturing and measurements. The vibration frequency from the environment is distributed at mainly less than 100 Hz, and the vibration level ranges to several tens of micrometers. To guarantee proper operation of precision instruments, the vibration regulations such as VC (vibration criteria) and those of NIST (National Institute of Standards and Technology) [1,2] require the transmitted vibrations to be below a certain level. A dual-chamber pneumatic

*Corresponding author. Tel.: +82 42 350 3024; fax: +82 42 350 8220.
E-mail address: kjkim@kaist.ac.kr (K.-J. Kim).

0022-460X/$ - see front matter © 2009 Elsevier Ltd. All rights reserved.
doi:10.1016/j.jsv.2008.12.028

Nomenclature

A	area (m^2)
$C(X_p,\omega)$	flow restriction coefficient $(ms)^{-1}$
$C_{eq}(X_p)$	equivalent flow restriction coefficient $(ms)^{-1}$
D_c	capillary tube diameter (m)
fr	friction coefficient for unidirectional flow
g	gravitational acceleration, 9.81 (m/s^2)
j	$\sqrt{-1}$
k	stiffness (N/m)
K	minor loss coefficient
L_c	capillary tube length (m)
m_p	payload mass (kg)
N	chamber volume ratio ($= V_{b0}/V_{t0}$)
p	pressure (N/m^2)
R	the universal gas constant ($= 286.9\,J/(kg\,K)$)
Re	Reynolds number
$s(=j\omega)$	Laplace operator
T	temperature (K)
u	cross-sectional mean fluid velocity (m/s)
V	volume (m^3)
V_{b0}	bottom chamber volume (m^3)
V_{t0}	top chamber volume (m^3)
X	dynamic amplitude (m)
η	loss factor
κ	the specific heat ratio ($= 1.4$)
μ	dynamic viscosity (Ns/m^2)
ρ	density (kg/m^3)
ω	excitation frequency (rad/s)
ω_{op}	resonance frequency of optimum transmissibility (rad/s)

Subscripts

0	static
atm	atmosphere
b	bottom chamber
c	capillary tube
D	diaphragm
eq	equivalent
max	maximum
p	piston
t	top chamber
s	single chamber
op	optimum

Superscripts

*	complex variable
-	cycle average

vibration isolator consisting of a dual-chamber pneumatic spring, which plays a key role in it, and a payload, as shown in Fig. 1, is generally accepted for this purpose. The dual-chamber pneumatic spring has two pneumatic chambers connected by a capillary tube. A rigid piston supports the payload including an isolation table and precision instruments. Additionally, a fiber-reinforced rubber diaphragm having a complicated

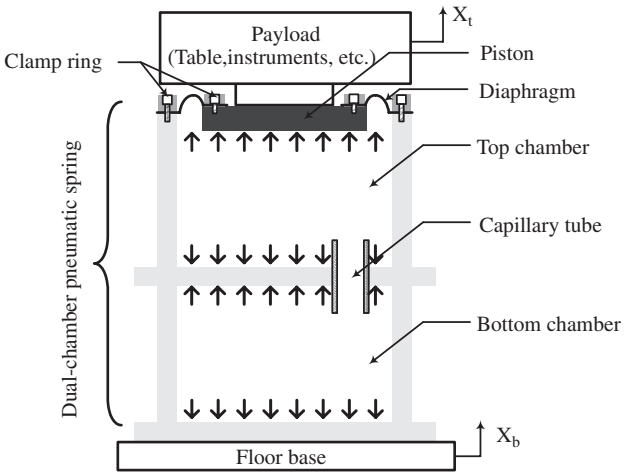

Fig. 1. Schematics of dual-chamber pneumatic vibration isolator consisting of dual-chamber pneumatic spring and payload. (Leveling valve is not shown in this figure.)

shape and held by a clamp ring is installed for prevention of air leakage. The internal air pressure to satisfy static-equilibrium with the payload can be automatically adjusted by a leveling valve (not shown in Fig. 1), which makes the pneumatic spring attractive as a vibration isolation component. The pneumatic springs, furthermore, can have a low stiffness due to the volumetric compressibility of air. This lends the pneumatic isolation system a low resonant frequency ranging between 1 and 3 Hz. In addition, the friction of air in the capillary tube across the dual-chambers provides sufficient damping in the isolation system.

As the environmental vibration regulations [1,2] for precision instruments become increasingly stringent, it is necessary to further improve the performance of pneumatic vibration isolation systems in a such way that the isolator should be capable of having a low resonance frequency and low transmissibility values at, and far above, the resonance frequency. Such improvements can be accomplished in a passive or active manner. In either case, precise modeling of the isolation system is the most important prerequisite. Some studies related to linear modeling of a pneumatic vibration isolator can be found in the literature [3–5]. However, the models of these previous studies have limitations in representing the amplitude-dependent behavior of the dual-chamber pneumatic spring investigated in our earlier research [6]. As detailed in Ref. [6], consideration of the nonlinear air flow through the capillary tube and the amplitude-dependent complex stiffness of the diaphragm improved the complex stiffness model of the dual-chamber pneumatic spring. This paper discusses a transmissibility design method of a pneumatic vibration isolator wherein an improved complex stiffness model of the dual-chamber pneumatic spring is employed.

As noted above, for better vibration isolation performance, the primary objective for the transmissibility design of a dual-chamber pneumatic vibration isolator should be focused on minimization of the peak value of transmissibility, i.e. the transmissibility at the resonance frequency, as well as the transmissibility in the high frequency range far above the resonance frequency. Although time-consuming numerical techniques can be employed to meet this design purpose, this paper attempted to exploit the frequency-dependent damping characteristics of the dual-chamber pneumatic spring. Noting that the loss factor of a pneumatic spring, given by the imaginary part divided by the real part of the complex stiffness and representing damping characteristics, generally exhibits a bell-shaped curve in the frequency domain [6], the peak transmissibility could be minimized by coinciding the frequency of the maximum loss factor with the resonance frequency of the transmissibility due to maximum utilization of damping at the resonance frequency.

Section 2 briefly reviews the complex stiffness model of the dual-chamber pneumatic spring developed in our previous research [6], and proposes a simple form of complex stiffness for transmissibility design. A clear problem definition for transmissibility design, including objective, constraints, and design variables, is provided in Section 3, which also covers the method for optimum transmissibility design. Section 4 then presents some experimental illustrations for validation of the proposed design method. Finally, this paper closes with conclusions in Section 5.

2. Complex stiffness model of dual-chamber pneumatic for transmissibility design

2.1. Summary for complex stiffness modeling of dual-chamber pneumatic spring in Ref. [6]

Consider again dual-chamber pneumatic spring shown in Fig. 1 to derive its complex stiffness defined as the force for unit displacement of the piston. Small piston movements caused by base vibrations will change mass, pressure, volume, and temperature of the air in upper chamber, cause the air to flow through the capillary tube, and consequently change mass, pressure, temperature in bottom chamber. Hence, complex stiffness of pneumatic spring is related to rigid body dynamics of the piston, thermodynamics in the pneumatic chambers and fluid dynamics across the capillary tube. Furthermore, as the diaphragm expands by the pressurized air, it plays indeed the role of another complex stiffness element in the pneumatic spring. Existing linear models [3–5] of dual-chamber pneumatic spring were not adequate for the characteristics of amplitude-dependent behavior of actual pneumatic spring observed in our previous research [6]. Taking two major considerations made an improvement for the complex stiffness model as follows. One is to consider the amplitude-dependent complex stiffness of diaphragm. The other is to use a nonlinear air flow model in capillary tube by the inclusion of minor pressure loss at the inlet- and outlet- of it. For convenience, the improved complex stiffness model of dual-chamber pneumatic spring depending on dynamic amplitude of piston X_p as well as frequency ω was

adopted from Ref. [6], and can be re-written in the following form;

$$k^*(X_p,\omega)=k_0\frac{1+\dfrac{V_{total}NC(X_p,\omega)}{RT_0\kappa(N+1)}\mathrm{j}\omega}{1+\dfrac{V_{total}NC(X_p,\omega)}{RT_0\kappa(N+1)^2}\mathrm{j}\omega}+k_D^*(X_p,\omega) \tag{1}$$

where

$$N=V_{b0}/V_{t0} \tag{2}$$

$$V_{total}=V_{t0}+V_{b0} \tag{3}$$

$$k_0=\kappa p_0 A_p^2/V_{total} \tag{4}$$

denote volume ratio of the bottom- to top-chamber volume (V_{b0}, V_{t0}), the total chamber volume, and the stiffness associated with the total chamber volume, respectively. In Eqs. (1) and (4), R (= 286.9 J/(kg K)) is the universal gas constant, T_0 temperature when the isolator reached to a static-equilibrium, κ(= 1.4) the specific heat ratio of air, p_0 the absolute chamber pressure, and A_p the equivalent piston area under the assumption that the movement of the piston and diaphragm can be approximated by that of an artificial piston. Amplitude- and frequency-dependent complex stiffness of diaphragm k_D^* (X_p,ω) can be indirectly estimated simply by subtracting stiffness of the pressurized air k_s(= $\kappa p_0 A_p{}^2/V_{t0}$) from measurement of the total complex stiffness for a single chamber pneumatic spring, which is formed by blocking the capillary tube. $C(X_p,\omega)$ in Eq. (1) resulting from the consideration of nonlinear air flow in capillary tube is given as below,

$$C(X_p,\omega)=\left(\frac{L_c}{D_c}fr(X_p,\omega)+K\right)\frac{4A_pX_p\omega}{3\pi A_c^2}\quad (\mathrm{ms})^{-1} \tag{5}$$

where L_c, D_c and A_c, respectively, represent length-, diameter- and cross-sectional area- of the circular capillary tube, K(= 1.5) the minor pressure loss coefficient for the description of dramatic pressure loss at the inlet- and outlet- of the capillary tube [7]. Finally, the unidirectional friction coefficient fr in Eq. (5) accounting for a frictional loss within capillary tube is the function of Reynolds number Re and given by [8]

$$\begin{aligned} fr&=\frac{64}{Re}\quad \text{for } Re\leqslant 2300 \text{ (laminar flow)}\\ &=\frac{0.3164}{Re^{1/4}}\quad \text{for } 4000\leqslant Re\leqslant 10^5 \text{ (turbulent flow)}\end{aligned} \tag{6}$$

where Reynolds number is defined as follows:

$$Re=\frac{\rho\bar{u}D_c}{\mu} \tag{7}$$

ρ and μ denotes the density- and dynamic viscosity- of air, respectively, $\bar{u}$ the cycle-averaged fluid velocity, i.e. computed by

$$\bar{u}=\frac{\omega}{2\pi}\int_0^{2\pi/\omega}|u|\,\mathrm{d}t=\frac{2A_p}{\pi A_c}\omega X_p \tag{8}$$

In Ref. [6], assuming that flow in the capillary tube under harmonic piston movements is oscillating, the frictional pressure loss was described by employing an oscillating friction coefficient [9,10] instead of unidirectional one [8], and the significance of minor pressure loss was under-valued. Recently, after the Ref. [6] was published, we have found that the so called minor pressure loss is not any more minor but as important as the frictional loss. Further, it has been found that the flow in the capillary tube must be treated as a unidirectional flow, not the oscillating one. These mistakes and corrections in adopting the flow type are stated in Appendix A.

Because $C(X_p,\omega)$ is inversely proportional to the mass flow rate in capillary tube, it will be designated as the flow restriction coefficient throughout this paper. Rigorously, the flow restriction coefficient $C(X_p,\omega)$ is not the

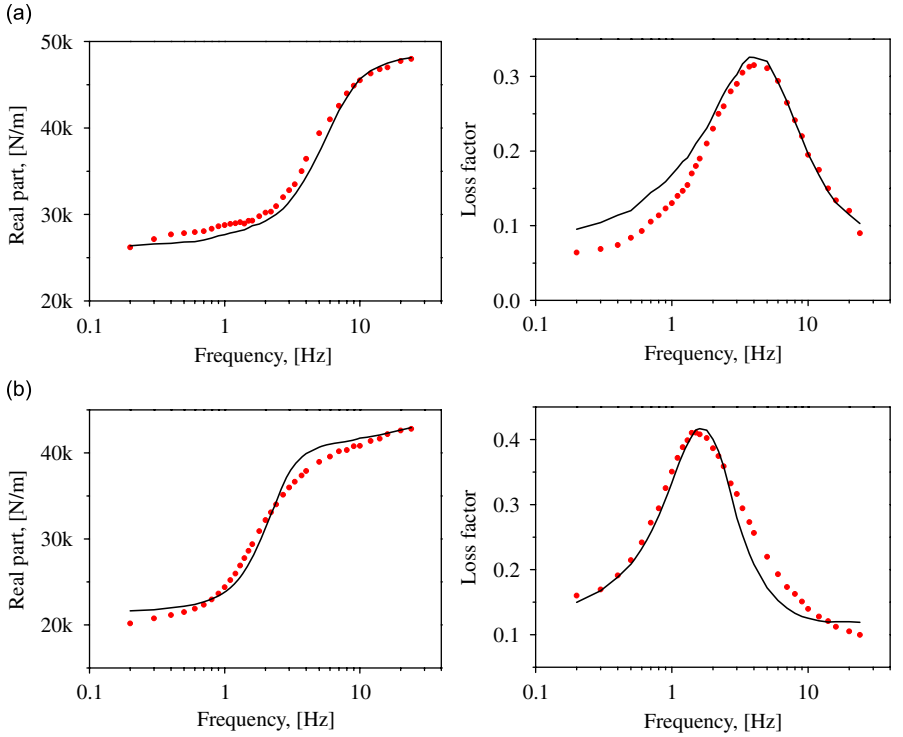

Fig. 2. Comparison between complex stiffness (k^*) by model and the one by measurements; real part: Re[k^*]; loss factor: Im[k^*]/Re[k^*]; (model: —, experiment: ●): (a) dynamic amplitude, $X_p = 10\,\mu m$ and (b) dynamic amplitude, $X_p = 100\,\mu m$.

damping coefficient of capillary tube, which has the dimension of [N/(m/s)]. However, the damping characteristics of capillary tube can still be represented or controlled by the flow restriction coefficient, since a simple multiplying ρA_c^2 and $C(X_p,\omega)$ together gives the damping coefficient of capillary tube. Hence $C(X_p,\omega)$ will be treated as a damping design parameter for transmissibility design.

By using Eqs. (1)–(8), the complex stiffness of dual-chamber pneumatic spring can be calculated for a given dynamic amplitude X_p and frequency ω. As shown in Fig. 2, the results in terms of real part representing elastic stiffness and loss factor given by the imaginary part divided by real part of the complex stiffness and representing damping characteristics are shown with experimental values for the dynamic amplitude cases of 10 and 100 μm, respectively. All parameter values used in the calculation are listed in Table 1 with physical dimensions of the pneumatic spring. It can be known from Fig. 2 that amplitude- and frequency-dependent behaviors of dual-chamber pneumatic spring are well predicted by our improved model. (Refer to Ref. [6] for more detailed discussion.)

2.2. Concept for transmissibility design via observing the complex stiffness of dual-chamber pneumatic spring

The primary objective of transmissibility design is to minimize the peak value of transmissibility, i.e. transmissibility at the resonance frequency, as well as the transmissibility in high frequency range far above the resonance frequency. Even though numerical techniques found in classical optimization theory [11] can be necessarily applied to satisfy such design objective, yet not only time-consuming numerical computations are inevitable but also no physical meaning is attainable. If we examine the loss factor of dual-chamber pneumatic spring, it generally exhibits a bell-shaped curve in frequency domain as schematically represented in Fig. 3. This means that energy-dissipation of dual-chamber pneumatic spring is most important around the frequency point of maximum loss factor $\omega_{loss\ factor:max}$, but is not in other frequency ranges. Although damping (or loss factor) varies with frequency, the role of damping would be significant around the resonance frequency [12]. Hence it is definitely desirable to maximize the loss factor of dual-chamber pneumatic spring at the resonance

Table 1
Design specifications of employed pneumatic spring.

Symbol	Name	Value
ρ	Density	5.97 (kg/m^3)
m_p	Payload mass	100 (kg)
μ	Dynamic viscosity	1.79×10^{-5} (Ns/m^2)
R	Gas constant	286.9 (J/(kg K))
κ	Specific heat ratio	1.4
T_0	Temperature	288.1 (K)
p_0	Supplied pressure	4.93×10^5 (Pa)
K	Minor pressure loss coefficient	1.5
V_{t0}	Top chamber volume	8.1×10^{-4} (m^3)
V_{b0}	Bottom chamber volume	1.5×10^{-3} (m^3)
N	Volume ratio, V_{b0}/V_{t0}	1.9
L_c	Capillary tube length	1.2×10^{-2} (m)
D_c	Capillary tube diameter	0.9×10^{-3} (m)
A_p	Effective piston area	5.3×10^{-3} (m^2)

Note: Complex stiffness of diaphragm $k^*_D(X_p,\omega)$ cannot be expressed with single value due to its dependence on the frequency as well as the dynamic amplitude. It can be found in Fig. 8 of Ref. [6], which was adopted in the present study.

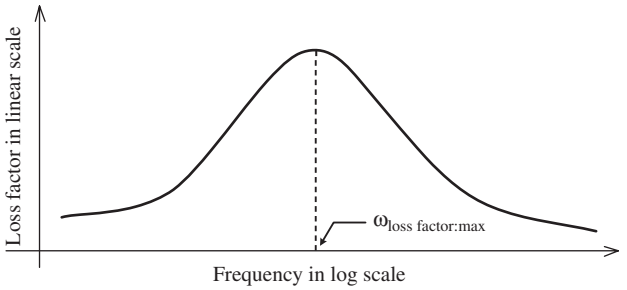

Fig. 3. Typical frequency-dependent behavior of loss factor of dual-chamber pneumatic spring.

frequency of pneumatic vibration isolator. In other words, once the frequency of maximum loss factor is adjusted to coincide with the resonance frequency of transmissibility, then we can exploit the damping of dual-chamber pneumatic spring as much as possible, i.e. minimization of the peak transmissibility is achievable.

In a single-degree of freedom vibration isolation system consisting of lumped mass (m) and Voigt element with the linear spring (k) and viscous damper (d) in parallel, the damping ratio $\zeta(=d/(2\sqrt{mk}))$ can adjust the peak value of transmissibility as shown in Figs. 4(a) and (b). However the effect of damping force appears in frequency ranges far higher than resonance frequency, because the loss factor of Voigt element ($=d\omega/k$) increases with frequency as represented in Fig. 5. Hence the change of ζ (or d) would result in the variation of transmissibility slope representing the isolation efficiency in the high frequency range. In case of dual-chamber pneumatic spring, loss factor of which approaches to '0' in the high frequency range, the transmissibility slope of pneumatic vibration isolator does not change greatly as the previous case even if the peak transmissibility is minimized. Such a merit of pneumatic vibration isolator can be found also in the dynamic systems with the standard linear solid element [13,14] consisting of a linear spring and Maxwell element in parallel as shown in Fig. 6. Consequently, while avoiding the conventional optimization technique, the basic strategy for optimum design can be established as making the frequency of maximum loss factor to coincide with the resonance frequency.

However deriving those two frequencies needs a differentiation of loss factor with respect to frequency. This cannot be done, since $C(X_p,\omega)$ is an implicit function of frequency. To avoid such a cumbrance in treating with $C(X_p,\omega)$, in the following section, equivalent flow restriction coefficient $C_{eq}(X_p)$ will be proposed by approximating $C(X_p,\omega)$ with $\omega C_{eq}(X_p)$. An explicit relation between $C_{eq}(X_p)$ and geometry of capillary tube will also be given throughout a parametric analysis.

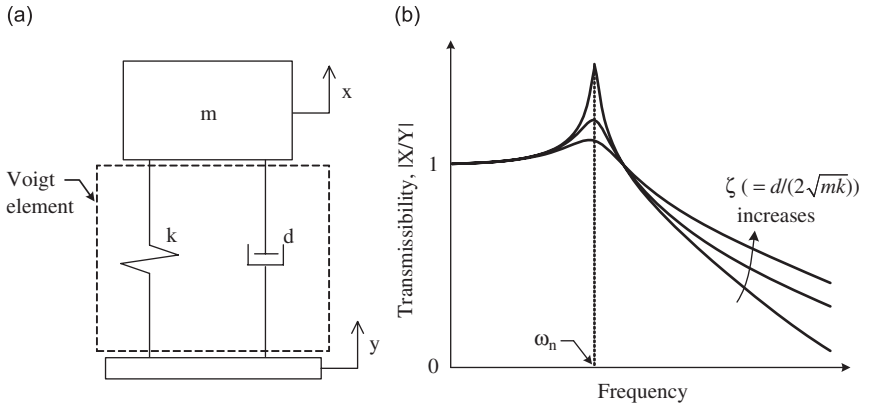

Fig. 4. Single degree of freedom vibration isolation system and its transmissibility: (a) single degree of freedom (dof) vibration isolation system with Voigt element and (b) transmissibilities of single dof system in (a).

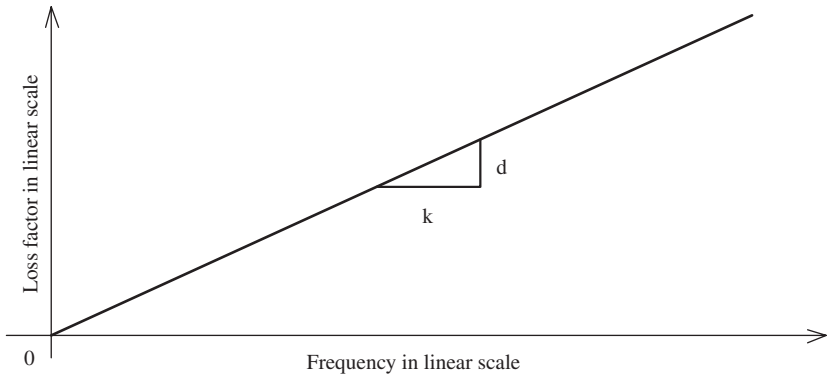

Fig. 5. Loss factor of Voigt element.

2.3. Approximation of flow restriction coefficient $C(X_p,\omega)$ by $\omega C_{eq}(X_p)$

Fig. 7 shows a calculation example of flow restriction coefficient $C(X_p,\omega)$ nearly exhibiting a linear increase with frequency. Hence if we approximate $C(X_p,\omega)$ by the product of frequency ω and the equivalent flow restriction coefficient $C_{eq}(X_p)$ through the least-square curve fitting, instead of leaving it as an implicit function of frequency, then complex stiffness model of dual-chamber pneumatic spring can be simply expressed as follows:

$$k^*(X_p,\omega) = k_0 \frac{1+\dfrac{V_{total}NC_{eq}(X_p)}{RT_0\kappa(N+1)}\mathrm{j}\omega^2}{1+\dfrac{V_{total}NC_{eq}(X_p)}{RT_0\kappa(N+1)^2}\mathrm{j}\omega^2} + k_D^*(X_p,\omega) \tag{9}$$

Dotted-line in Fig. 8 shows a complex stiffness calculation example with $\omega C_{eq}(X_p)$ for a specific dynamic amplitude of 50 μm. Even though the loss factor calculated with $\omega C_{eq}(X_p)$ exhibits some discrepancies to the one with $C(X_p,\omega)$, overall characteristics of complex stiffness are well matched between those two models. Hence it can be emphasized that the simple complex stiffness model with $\omega C_{eq}(X_p)$ can describe the stiffness- and damping-characteristics of dual-chamber pneumatic spring as faithfully as the one with $C(X_p,\omega)$.

Although computational loads in the calculation of complex stiffness are significantly decreased by introducing $\omega C_{eq}(X_p)$ instead of $C(X_p,\omega)$, bottleneck is missing the explicit relation between geometric design variables of capillary tube and $C_{eq}(X_p)$, which would be extremely desirable at the stage of capillary tube design. In order to obtain such a quantitative relation, following parametric studies were conducted.

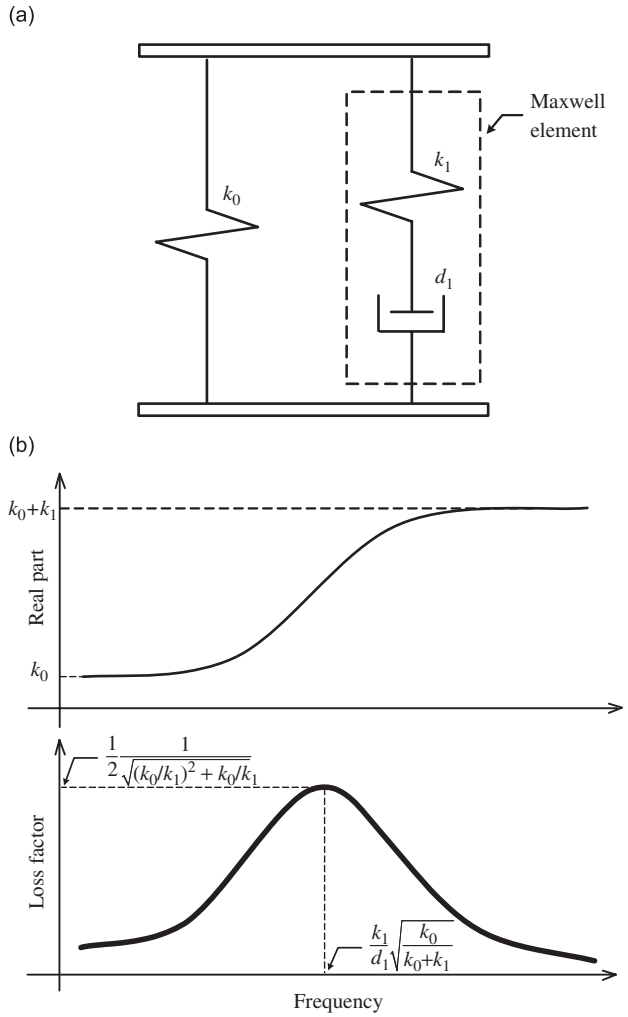

Fig. 6. Standard linear solid model: (a) mechanical model of standard linear solid: linear spring and Maxwell element in parallel and (b) complex stiffness of the above ($= k_0+k_1 j\omega/(j\omega+k_1/d_1)$).

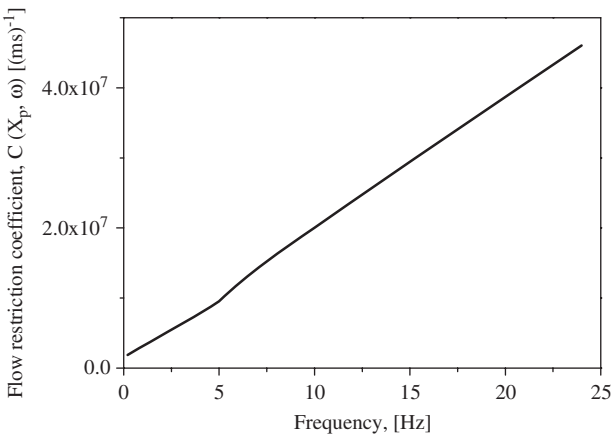

Fig. 7. Calculation example of flow restriction coefficient $C(X_p,\omega)$: dynamic amplitude, $X_p = 50\,\mu m$.

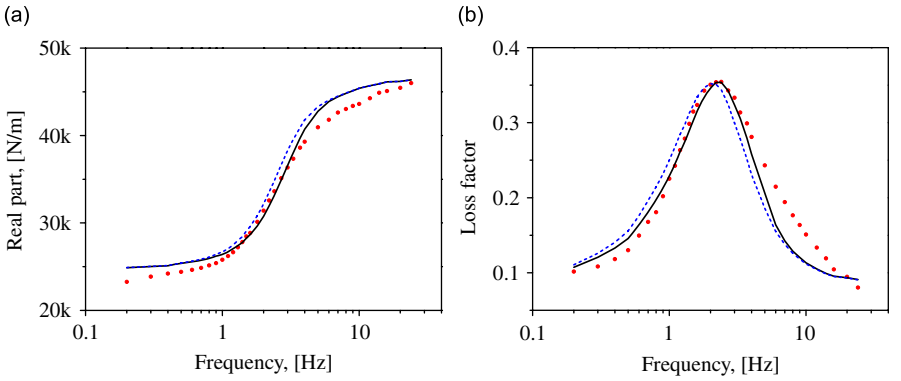

Fig. 8. Approximation of flow restriction coefficient $C(X_p,\omega)$ by $\omega C_{eq}(X_p)$ in complex stiffness calculation: dynamic amplitude, $X_p = 50\,\mu m$; (complex stiffness model with $C(X_p,\omega)$: —, complex stiffness model with $\omega C_{eq}(X_p)$: ·····, experiment: ●): (a) real part: Re[k^*] and (b) loss factor: Im[k^*]/Re[k^*].

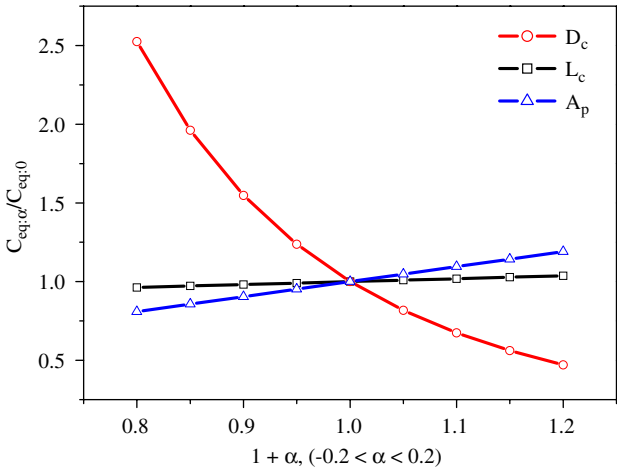

Fig. 9. Parametric study results of equivalent flow restriction coefficient C_{eq} with respect to geometric design variables of capillary tube length (L_c), diameter (D_c), piston area (A_p), and dynamic amplitude, $X_p = 50\,\mu m$; (D_c: —○—, L_c: –□–, A_p: —△—).

By referring to Eq. (5), diameter D_c and length L_c of capillary tube and equivalent piston area A_p were selected as parameters for $C_{eq}(X_p)$. Then, for a given dynamic amplitude X_p, i.e. 50 μm, variations of $C_{eq}(X_p)$ were evaluated while varying each parameter from −20 percent to +20 percent by increment of α percent. The results are shown in Fig. 9, where $C_{eq:0}(= 5.87\times10^5\,m^{-1})$ is the constant obtained for a set of reference values of parameters, i.e. $D_{c:0} = 0.9\,mm$, $L_{c:0} = 12\,mm$, $A_{p:0} = 5.3\times10^{-3}\,m^2$, $X_{p:0} = 50\,\mu m$ and $C_{eq:\alpha}$ denotes the one when the variation of α was made for each parameter. Repeating above parametric study with respect to dynamic amplitude X_p gives the result in Fig. 10. By combining the simulation results in Figs. 9 and 10 through curve-fitting, one can obtain the quantitative relation between $C_{eq}(X_p)$ and the geometry variables of capillary tube as the following non-dimensional form,

$$\frac{C_{eq}(X_p)}{C_{eq:0}} = \left(\frac{D_c}{D_{c:0}}\right)^{-4.14}\left(\frac{L_c}{L_{c:0}}\right)^{0.18}\left(\frac{A_p}{A_{p:0}}\right)^{0.95}\left(\frac{X_p}{X_{p:0}}\right)^{0.95} \tag{10}$$

The rms errors between the original C_{eq} and the approximated one for each design parameter (D_c, L_c, A_p) and dynamic amplitude (X_p) are far less than 1 percent as presented in Table 2. However, the parametric representation of $C_{eq}(X_p)$ should be validated through an experiment. To this end, complex stiffness measurements of dual-chamber pneumatic spring having a modified geometry of capillary tube ($D_c = 0.8\,mm$,

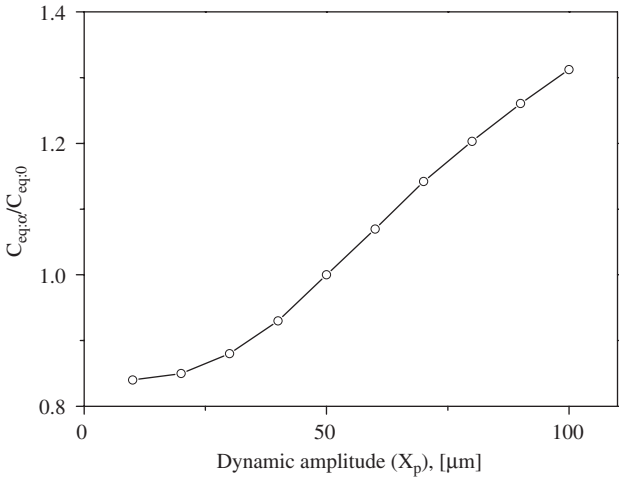

Fig. 10. Parametric study results of equivalent flow restriction coefficient C_{eq} with respect to dynamic amplitude X_p.

Table 2
The rms-errors[a] between the original C_{eq} and the approximated one for each design parameter (D_c, L_c, A_p) and dynamic amplitude (X_p).

	D_c	L_c	A_p	X_p
rms error (percent)	0.13	0.08	0.11	0.31

[a]rms error $= \sum_{i=1}^{n} \frac{(\text{Approximated } C_{eq})_i - (\text{Original } C_{eq})_i}{(\text{Original } C_{eq})_i} \times 100\,(\%)$, $n =$ number of data point.

$L_c = 30$ mm) were compared to the simple model calculated with Eqs. (9) and (10). As shown in Fig. 11, the measurement data are quite well predicted by the simple model. Similarly to the case of Fig. 8, prediction for loss factor shows some discrepancies with the experimental measurements in the low- and high-frequency ranges, but the values of maximum loss factor and stiffness characteristic in the low- and high-ranges are well matched between model and experiment. Besides the simple complex stiffness model predicts well the amplitude dependency of dual-chamber pneumatic spring. The average values of root mean square errors between model and measurement for various input levels are 3 percent for real part and 6 percent for loss factor, respectively, both which are satisfactory. Hence the simple complex stiffness model (Eq. (9)) together with Eq. (10) can be efficiently adopted for transmissibility design of dual-chamber pneumatic vibration isolator in the following section.

3. Method of transmissibility design

3.1. Problem definition for transmissibility design

For a design minimizing the peak transmissibility and the transmissibility in high frequency range, two design constraints in the following should be firstly provided. One is the payload mass m_p determined by the specification of the precision machine tools on the table. Often, pneumatic springs are equipped with precision instruments which have several supporting machines (for example, cooling-pump, fan, and etc.) for its proper operation. So there would not be enough space for air springs, because such vibration-generating equipments together with air springs should be placed underneath the table. The other constraint, hence, can be the installation space of isolator, i.e. the total chamber volume V_{total} of pneumatic spring formed by the height from floor to payload and the size of payload.

By referring to Eq. (9), the stiffness of total chamber volume k_0, the chamber volume ratio N and the flow restriction coefficient $C(X_p,\omega)$ relating damping characteristics of capillary tube can be considered as the design variables of dual-chamber pneumatic spring together with the complex stiffness of diaphragm k_D^*.

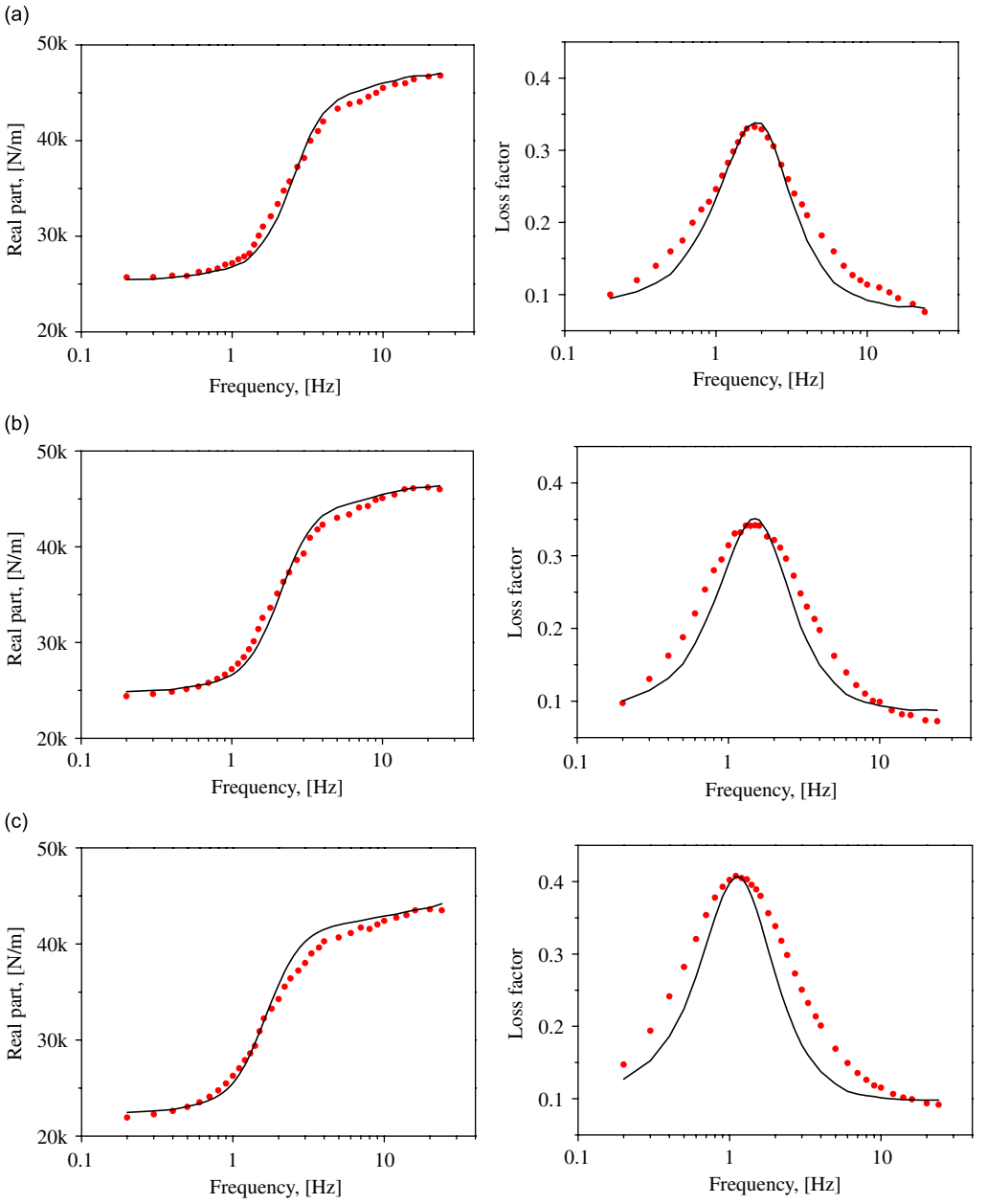

Fig. 11. Complex stiffness measurements by modifying the capillary tube geometry ($D_c = 0.8$ mm, $L_c = 30$ mm) and comparison to simple model with equivalent flow restriction coefficient $C_{eq}(X_p)$; (model: —, experiment: ●) real part: Re[k^*]; loss factor: Im[k^*]/Re[k^*]: (a) dynamic amplitude, $X_p = 30$ μm, (b) dynamic amplitude, $X_p = 50$ μm and (c) dynamic amplitude, $X_p = 70$ μm.

For the cases of supplied air pressure p_0 and equivalent piston area A_p related together to the stiffness of total chamber by Eq. (4), they are both determined from the condition of static-equilibrium with the payload as follows (in actual operations, leveling valves automatically adjust the air pressure to maintain a static-equilibrium):

$$m_p g = A_p(p_0 - p_{atm}) \tag{11}$$

where $g(= 9.81\,\mathrm{m/s^2})$ denotes the gravitational acceleration, $p_{atm}(= 101.325\,\mathrm{kPa})$ the atmospheric pressure. Given the payload mass, infinite number of combinations between p_0 and A_p satisfying static-equilibrium

would be possible. However, modification of A_p would basically accompany change of the diaphragm, making the design modification of pneumatic spring to be complex. In the present study, A_p was not changed from the current design specification, which consequently determines p_0. Hence, both p_0 and A_p were not considered as design variables in the present study. If one considers further that the total chamber volume V_{total} is given as a constraint, the stiffness of total chamber volume k_0 can be regarded as a constant. Accordingly, the chamber volume ratio N can only be considered as design variable for air stiffness, while excluding k_0.

Then the transmissibility design problem for pneumatic vibration isolator can be briefly summarized in the following way:

- Design objective: minimize the transmissibility at resonance frequency as well as in higher frequency range.
- Constraints: the total chamber volume of pneumatic spring $V_{total}(=V_{b0}+V_{t0})$ and the payload mass m_p are given.
- Design variables: chamber volume ratio N, flow restriction coefficient $C(X_p,\omega)$, complex stiffness of diaphragm $k_D^*(X_p,\omega)$.

3.2. Optimum transmissibility of dual-chamber pneumatic vibration isolator without diaphragm

3.2.1. Transmissibility model without diaphragm

Since the complex stiffness model of dual-chamber pneumatic spring has dependencies on not only frequency but also amplitude, the transmissibility model of pneumatic vibration isolator is basically amplitude-dependent. Hence, at each frequency point, the dynamic amplitude of piston X_p representing the relative displacement between the table and the base should be determined beforehand by means of an iterative calculation such as Newton–Raphson method. Furthermore nonlinear analysis technique of harmonic balance method might be required to obtain transmissibility of a system with amplitude- and frequency-dependent parameters [15], which is far beyond our research scope. Our primary concern is to develop a *simple* strategy for transmissibility design rather than to compute rigorously via the time-consuming nonlinear analysis technique. For this purpose, we will assume that dynamic amplitude is constant with frequency, given by $\bar{X}_p$, to eliminate the amplitude-dependency in complex stiffness model $K^*(X_p,\omega)$. This assumption seems to be cruel, because the floor vibration amplitude for typical floor falls off dramatically with increased frequency, and the payload motion far above the resonance frequency decreases as frequency increases. However, considering that narrow frequency band around the resonance is of interest, and amplitude-dependency of complex stiffness of pneumatic spring is not significant in the high frequency range, the assumption of constant target amplitude $\bar{X}_p$ was adhered.

Regarding the dynamic amplitude of piston X_p as constant, the assumption of quasi-linear system [16] for the dual-chamber pneumatic vibration isolator shown in Fig. 1 gives the following transmissibility model:

$$\frac{X_t(\omega)}{X_b(\omega)}=\frac{k^*(\omega)}{-m_p\omega^2+k^*(\omega)}$$
$$=\frac{\mathrm{j}[k_0(N+1)+k_D^*]\omega^2+(k_0+k_D^*)\dfrac{(N+1)^2}{\alpha N}}{-\mathrm{j}m_p\omega^4+\left(\mathrm{j}[k_0(N+1)+k_D^*]-\dfrac{m_p(N+1)^2}{\alpha N}\right)\omega^2+(k_0+k_D^*)\dfrac{(N+1)^2}{\alpha N}} \tag{12}$$

where X_t and X_b are the displacement- of payload and floor, respectively, and α given by the following:

$$\alpha=\frac{V_{total}C_{eq}(\bar{X}_p)}{RT_0\kappa} \tag{13}$$

We have rather a complicated form of transmissibility higher than fourth order due to the frequency-dependent behavior of diaphragm complex stiffness. However, method of transmissibility design can be proposed by neglecting the complex stiffness of diaphragm in Eq. (12), since the frequency dependence of

diaphragm complex stiffness is relatively simple than that of air. This allows Eq. (12) to be in a simpler form as

$$\frac{X_t(\omega)}{X_b(\omega)} = \frac{\mathrm{j}k_0(N+1)\omega^2 + k_0\dfrac{(N+1)^2}{\alpha N}}{-\mathrm{j}m_p\omega^4 + \left(\mathrm{j}k_0(N+1) - \dfrac{m_p(N+1)^2}{\alpha N}\right)\omega^2 + k_0\dfrac{(N+1)^2}{\alpha N}} \tag{14}$$

3.2.2. Proposal for optimum transmissibility

Recalling that our basic strategy for transmissibility design is to coincide the frequency of maximum loss factor with the resonance frequency of transmissibility for maximum utilization of damping, such a condition for matching those two frequencies can be found as follows.

First, real part Re[k^*]- and loss factor $\eta[k^*]$- of dual-chamber pneumatic spring without diaphragm can be expressed as Eqs. (15) and (16), respectively:

$$\mathrm{Re}[k^*(\bar{X}_p,\omega)] = k_0\frac{1+(\alpha N)^2\omega^4/(N+1)^3}{1+(\alpha N)^2\omega^4/(N+1)^4} \tag{15}$$

$$\eta[k^*(\bar{X}_p,\omega)] = \frac{\mathrm{Re}[k^*(\overline{X}_p,\omega)]}{\mathrm{Im}[k^*(\overline{X}_p,\omega)]} = \frac{\alpha N^2\omega^2/(N+1)^2}{1+(\alpha N)^2\omega^4/(N+1)^3} \tag{16}$$

By letting that the first derivative of Eq. (16) with respect to frequency is equal to '0', the frequency of maximum loss factor $\omega_{loss\ factor:max}$ can be obtained as follows:

$$\frac{\partial\eta[k^*(\bar{X}_p,\omega)]}{\partial\omega} = 0 \rightarrow \omega_{loss\ factor:max} = \frac{(N+1)^{3/4}}{\sqrt{N\alpha}} = \frac{(N+1)^{3/4}}{\sqrt{NCV_{total}/RT_0\kappa}} \tag{17}$$

Then, the resonance frequency of transmissibility ω_{op} can be derived by using the stiffness value at the frequency of maximum loss factor and payload mass m_p. That is

$$\omega_{op} = \sqrt{\frac{\mathrm{Re}[k^*(\bar{X}_p,\omega_{loss\ factor:max})]}{m_p}} = \sqrt{\frac{2k_0(N+1)}{m_p(N+2)}} \tag{18}$$

Equalizing above two equations yields the value $C_{eq}(\bar{X}_p)$ that gives maximum damping design, say $C_{eq,op}(\bar{X}_p)$,

$$C_{eq,op}(\bar{X}_p) = \frac{RT_0\kappa}{2k_0V_{total}}m_p(1+2/N)\sqrt{1+N} \tag{19}$$

Hence, with the value of $C_{eq}(\bar{X}_p)$ satisfying $C_{eq,op}(\bar{X}_p)$, the peak transmissibility will be minimized for any value of chamber volume ratio N without degrading the transmissibility slope in the high frequency range. That is why subscripts '*op*', meaning of which is optimum, were used in Eqs. (18) and (19). In addition, we will designate the Eq. (19) as the optimum damping tuning condition.

However, it needs to confirm whether the optimum damping condition $C_{eq,op}(\bar{X}_p)$ can minimize the peak transmissibility without any great change of transmissibility slope as we have expected. To this purpose, a set of transmissibility curves obtained by varying $C_{eq}(\bar{X}_p)$ from zero to infinite are shown in Fig. 12, where the target dynamic amplitude $\bar{X}_p$ was assumed to be 50 μm and the chamber volume ratio N 1.9. Significant changes of peak transmissibility together with resonance frequency can be observed from the figure. Zero value of $C_{eq}(\bar{X}_p)$, implying no flow restriction of the capillary tube, corresponds to the configuration with no capillary tube, e.g. single-chamber pneumatic spring with the effective volume of both top- and bottom-chamber. Thus we have an undamped single degree of freedom vibration isolation system with resonance frequency in Eq. (20), while peak transmissibility approaches to infinite at this frequency.

$$\omega_n|_{C_{eq}(\bar{X}_p)=0} = \sqrt{k_0/m_p} \tag{20}$$

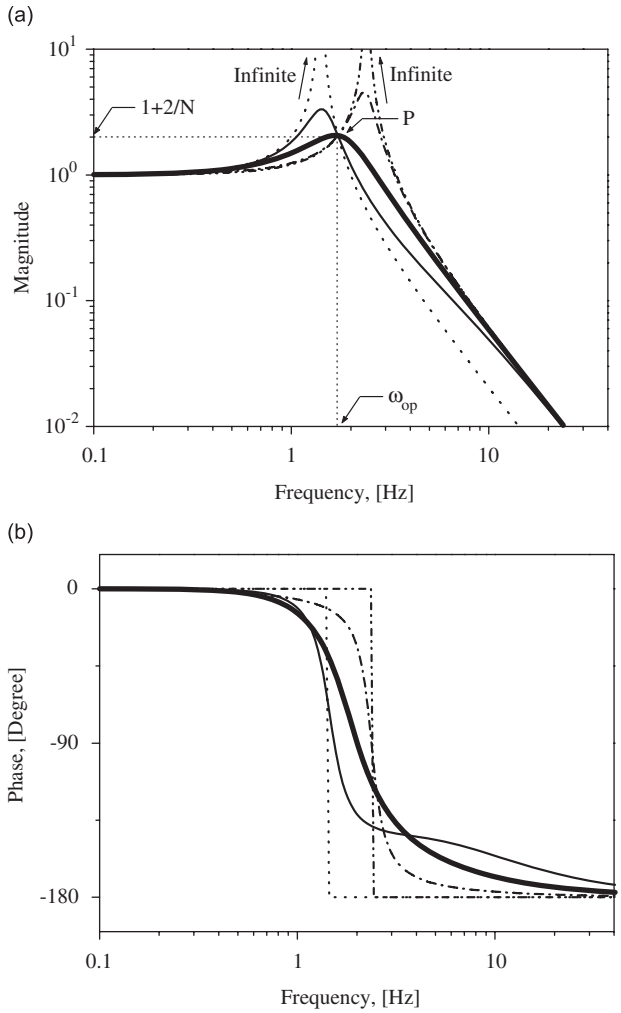

Fig. 12. Effects of equivalent flow restriction coefficient $C_{eq}(\bar{X}_p)$ on transmissibility for a specific value of chamber volume ratio, dynamic amplitude $\bar{X}_p = 50\,\mu m$, chamber volume ratio $N = 1.9$: (a) magnitude and (b) phase (C_{eq} = zero: ....., $C_{eq} = 5.87 \times 10^5$ (initial design): ——, $C_{eq} = 10.5 \times 10^5$ ($= C_{eq,op}$): ——, $C_{eq} = 40.1 \times 10^5$: — · —, C_{eq} = infinite: — · · —).

On the contrary, if $C_{eq}(\bar{X}_p)$ becomes an infinite, corresponding to blocked capillary tube, we again have an undamped single degree of freedom vibration isolation system but with effective volume of top chamber only. Owing to decreased effective chamber volume, the resonance frequency shown in Eq. (21) becomes higher than the case when $C_{eq}(\bar{X}_p) = 0$.

$$\omega_n|_{C_{eq}(\bar{X}_p)=\infty} = \sqrt{k_0(N+1)/m_p} > \omega_n|_{C_{eq}(\bar{X}_p)=0} \tag{21}$$

When $C_{eq}(\bar{X}_p)$ satisfies the optimum condition $C_{eq,op}(\bar{X}_p)$, we can convince that minimization of peak transmissibility was achieved, and that transmissibility slope does not exhibit any significant change after minimization as illustrated with thick line in Fig. 12. Therefore, the optimum condition $C_{eq,op}(\bar{X}_p)$ in Eq. (19) can be proved to be very valid. For reference, the peak value of optimum transmissibility given in Eq. (22) is expressed by the function of N only,

$$\left|\frac{X_t}{X_b}\right|_{\omega_{op}} = 1 + \frac{2}{N} \quad (>1 \text{ for any value of } N \text{ less than infinity}) \tag{22}$$

Meanwhile, it is interesting to note that all curves in Fig. 12 pass through a common point P regardless of $C_{eq}(\bar{X}_p)$. Exploiting this feature can derive the same optimum condition with Eq. (19). That is, once the

frequency point of P is given, imposing the condition that the slope of transmissibility at that frequency point is set to zero will result in the optimum condition of $C_{eq}(\bar{X}_p)$. The frequency point of P, which can be obtained by equating the equations of $|X_t/X_b|$ for $C_{eq}(\bar{X}_p)=0$ and ∞, becomes to be identical to ω_{op} in Eq. (18). Substitution ω_{op} into the frequency derivative of $|X_t/X_b|$ equated to zero is made, then the result will be also identical to $C_{eq}(\bar{X}_p)$ in Eq. (19). Since two ways of different approach yield the same results, the optimum condition $C_{eq,op}(\bar{X}_p)$ can be validated once again.

The derivation procedure for optimum damping tuning condition mentioned above quite resembles with the one of Den Hartog's dynamic vibration absorber [17] and Lanchester vibration damper [18], both which have *unique* solution for their absorber- and damper-value, respectively. On the other hand, the solution for the case of dual-chamber pneumatic vibration isolator is *not unique*, because we have only one design objective that minimizes the peak transmissibility under two design variables N and $C_{eq}(\bar{X}_p)$. We have just obtained an optimum relation between them. This naturally leads to the observations for variation of optimum transmissibility with respect to N.

3.2.3. *Optimum transmissibility variation with respect to the chamber volume ratio N*

To begin with, considering the constraint of total chamber volume V_{total}, transmissibility curves shown as solid lines in Fig. 13 were obtained by varying N while the capillary tube is blocked. Solid line (1) is especially the transmissibility by excluding the capillary tube, representing the behavior of undamped single degree of freedom vibration isolation system with the effective volume of given total chamber one. Varying N, i.e. dividing the total chamber volume as well as blocking the capillary tube gives again undamped single degree of freedom vibration isolation system due to the excluded damping of capillary tube. The resonance frequency increases with the increase of N, since the stiffness of single-chamber pneumatic spring is inversely proportional to its chamber volume. This is illustrated as solid lines (2) and (3) in Fig. 13, showing intersection with line (1) at P_1 and P_2, respectively. By referring to Fig. 12, all the transmissibility curves for a given N have a common intersection point regardless of $C_{eq}(\bar{X}_p)$. Such an intersection will travel on line (1) for any value of N, like P_1 and P_2. Hence we can obtain the optimum transmissibility as dotted lines (4) or (5) by using optimum damping tuning condition $C_{eq,op}(\bar{X}_p)$ for a given N or in such way that the slopes of transmissibility at the intersections P_1 and P_2, respectively, are equated to zero.

With increase of N, we can observe that the resonance frequency of optimum transmissibility ω_{op} increases, while the peak transmissibility decreases. Although the magnitude of transmissibility in higher frequency range, where the vibration isolation actually occurs, is enlarged with increase of N, the slope of optimum transmissibility does not change. Besides one should note that the resonance frequency of optimum transmissibility ω_{op} cannot be below $\omega_{n,min}$ unless the given total chamber volume increases, where $\omega_{n,min}$ in

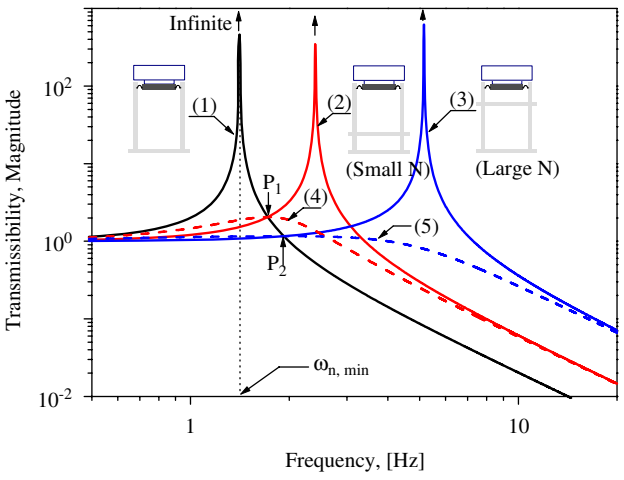

Fig. 13. Change of transmissibility according to chamber volume ratio N.

the following is the resonance frequency of transmissibility by excluding the capillary tube.

$$\omega_{n,min}(=\omega_n|_{C_{eq}(\bar{X}_p)=0}) = \sqrt{k_0/m_p} \tag{23}$$

Fig. 14 exhibits a set of optimum transmissibilities obtained by varying N under the given total chamber volume. We can easily recognize previously mentioned trade-offs among the resonance frequency, peak transmissibility and transmissibility in high frequency range, which are also summarized in Table 3. That is, both ω_{op} and the transmissibility in high frequency range should be dealt with the peak transmissibility. Ideally, it would be desirable to reduce all of the resonance frequency, peak transmissibility, and transmissibility in high frequency range for vibration isolation purpose, but which cannot be met under the given total chamber volume. Therefore practical transmissibility design for pneumatic vibration isolator should be negotiated with consideration of the above trade-off relationship and of the required isolation performance, simultaneously. Small N, for example, would be advantageous for reducing the resonance frequency. Meanwhile a faster settling time of transient response induced by impulsive load on the payload requires rather a large N, since damping will be increased by the decrement of peak transmissibility. To compromise such a conflict requirement for N, a determination of N or its tolerable range should be preceded from the negotiation between the resonance frequency and the settling time, followed by the design of optimum transmissibility using the optimum damping tuning condition in Eq. (19). Hence designer's decision with consideration of trade-off relationship mentioned above is inevitable for the selection of optimum transmissibility satisfying the requirement of isolation performance.

3.3. Negative effects of diaphragm stiffness on transmissibility design

Up to now, an optimum transmissibility design method for pneumatic vibration isolator was discussed without considering the complex stiffness of diaphragm, the effect of which will be detailed in this section.

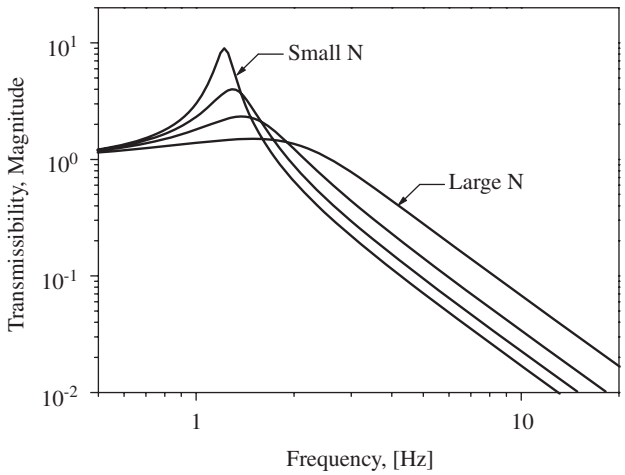

Fig. 14. Variation of optimum transmissibilities with respect to chamber volume ratio N under the given total chamber volume V_{total}.

Table 3
Trade-off among the resonance frequency-, peak transmissibility- and transmissibility in high frequency range- of optimum transmissibility with respect to chamber volume ratio N.

	$N\uparrow$	$N\downarrow$
Resonance frequency	↑	↓
Peak transmissibility	↓	↑
Transmissibility in high frequency range	↑	↓

Although the damping of diaphragm needs to be carefully treated with the stiffness of diaphragm, it is extremely difficult to realize the damping modification of diaphragm. On the other hand, the diaphragm stiffness can be rather easily done by shape design of diaphragm or by replacing with a different material. Besides we have found that stiffness of diaphragm greatly affects to the performance of pneumatic vibration isolator. Hence only the effect of diaphragm stiffness will be treated in the present study.

For our case [6], frequency-averaged stiffness of diaphragm is about 1.2 times higher than the one of air in pneumatic chamber. This ratio is quite similar to the one in Ref. [5]. The stiffness of diaphragm hence results in a rather higher resonance frequency than the theoretically calculated one without the diaphragm stiffness. Then such a high stiffness of diaphragm can be an obstacle in decreasing the resonance frequency of pneumatic vibration isolator.

It was previously mentioned that reducing the resonance frequency of optimum transmissibility was limited by the given total chamber volume. However, by neglecting the given constraint, i.e. by assuming that the total chamber volume can be increased, change of resonance frequency was calculated with- and without- the diaphragm stiffness as solid- and dashed-lines, respectively, shown in Fig. 15. According as the total volume increases, the resonance frequency in both cases decreases monotonically, but the case without diaphragm stiffness shows a more dramatic decrement than the one with diaphragm. For example, if the total volume is increased by three times of the current design, the resonance frequency without the diaphragm can be decreased by 0.52 Hz from 1.39 to 0.87 Hz. But the diaphragm stiffness diminishes such an improvement by only 0.26 Hz from 2.40 to 2.14 Hz. Although the zero resonance frequency is theoretically possible with an infinite total chamber volume provided that the stiffness of diaphragm is neglected, the resonance frequency with inclusion of diaphragm stiffness cannot be below 2.0 Hz. From these results originated by the larger stiffness of diaphragm than the one of air, one can see how the stiffness of diaphragm plays a negative role in decreasing the resonance frequency. Thus, decreasing the stiffness of diaphragm would be definitely beneficial for the decrement of resonance frequency and for reflecting the effect of increasing total chamber volume as well. For this purpose, calculation technique of diaphragm stiffness with FE code [19] can be helpfully employed for the shape design of diaphragm, but which will not be treated in this study.

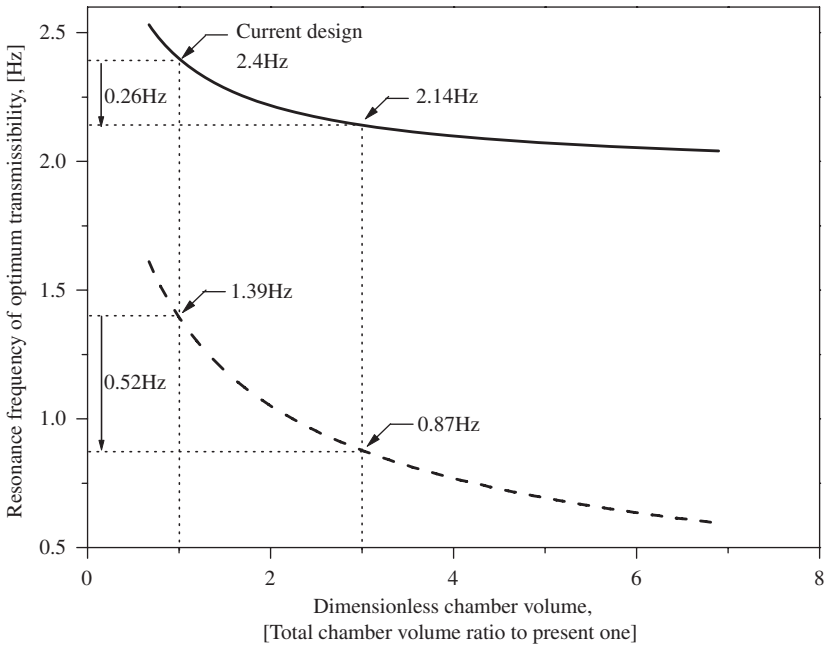

Fig. 15. Variation of resonance frequency of optimum transmissibility with respect to chamber volume (stiffness of diaphragm included: ——, stiffness of diaphragm excluded: ------).

3.4. Summary of step-by-step transmissibility design strategies

For the transmissibility design problem of dual-chamber pneumatic vibration isolator discussed so far, design strategies can be summarized as the following steps, experimental illustration of which will be given in the following section:

(i) Determine A_p by considering payload mass m_p and supply air pressure p_0. Determine also total chamber volume V_{total} by considering allowable space under the pneumatic table: Eq. (11).
(ii) Determine chamber volume ratio N by trading off between allowable peak transmissibility value $(1+2/N)$ at resonance frequency and value of transmissibility required at operating frequencies.
(iii) Determine optimum equivalent flow restriction constant $C_{eq,op}(\bar{X}_p)$ based on optimum damping tuning condition: Eq. (19).
(iv) Identify the ground or piston excitation level $\bar{X}_p$ and determine geometry of capillary tube based on Eq. (10) which yield the above $C_{eq,op}(\bar{X}_p)$.
(v) Decrease the diaphragm stiffness.

4. Experimental illustrations of proposed design method

4.1. Experimental procedure

Fig. 16 shows apparatus for an illustration of the proposed transmissibility design method. When the vibration exciter (Model: B&K 4826) is directly connected to the pneumatic vibration isolator, large level of floor vibration more than hundreds of micrometer are applied to the isolator. Hence an additional pneumatic bench-top with the payload mass of 400 kg, on which the pneumatic vibration isolator of interest was mounted, was employed to exploit its large inertia. To prevent unstable tilting motion of payload, its mass center was positioned lower than the connection point with dual-chamber pneumatic spring.

With the sampling frequency of 256 Hz, random signals having the frequency components between 0.5 and 30 Hz were produced by signal generator included in the computer-controlled dynamic signal analyzer (Model: B&K PULSE system), and passed to the vibration exciter through the power amplifier (Model: B&K 2721). Two signals from the high-sensitivity seismic accelerometers (Model: PCB 393B05, Sensitivity: 10 V/g) installed at the top- and bottom- of pneumatic vibration isolator passed through signal conditioner (Model: PCB 441A42) and post-processed to attain the transmissibility in the following,

$$Transmissibility = \frac{G_{X_b X_t}}{G_{X_b X_b}} \tag{24}$$

where X_t and X_b denote the acceleration signals from top- and bottom- of isolator, respectively, G_{XbXt} and G_{XbXb} the cross- and auto-PSD (power spectral density) [20] for the measured signals. Transmissibility was estimated by applying Hanning window under ensemble average of 50 times, and observed with the frequency resolution of 3.125×10^{-2} Hz.

Because the four pneumatic legs are connected by a tie-bar in H-shape for easy-movement and quick-installation purpose, but which is not shown in Fig. 16, the vibration exciter could not be precisely installed at the center of additional pneumatic bench-top, but slightly off the center. Although it may be claimed about the excitation of horizontal direction, the input power for horizontal direction is much lower than the one for vertical direction as shown in Fig. 17. The rms value of vertical input is approximately 100 times larger than the one of horizontal input. Hence the influence of horizontal input can be neglected although it dwells in the interested frequency ranges. Further one may not need to concern about the quality of experimental data due to the evanescent input power in low frequency range lower than 4 Hz, since coherence between X_t and X_b shown in Fig. 18 reaches almost one over the entire frequency range.

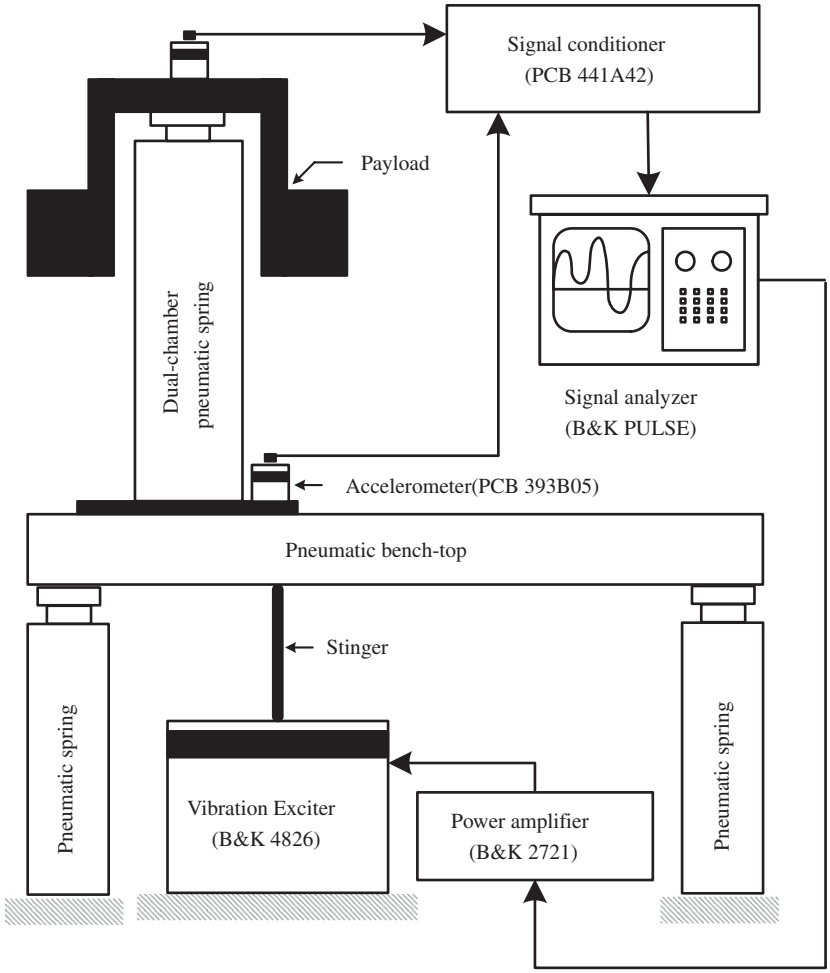

Fig. 16. Experimental set-up for transmissibility measurement of dual-chamber pneumatic vibration isolator.

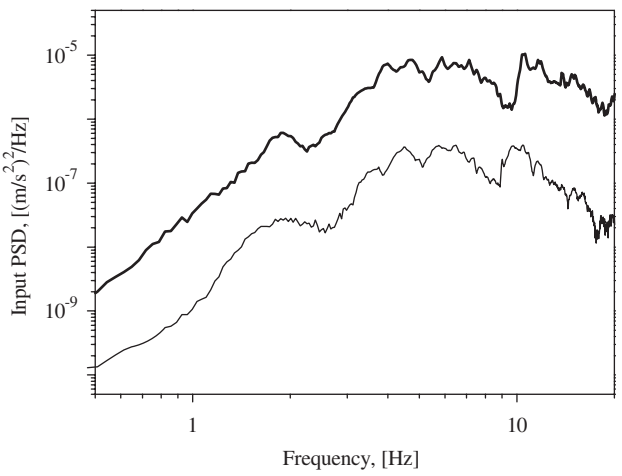

Fig. 17. Power spectral density of input signals; Hanning windowed, number of averages: 50, frequency resolution: 3.125×10^{-2} Hz (vertical direction: ——, horizontal direction: ——).

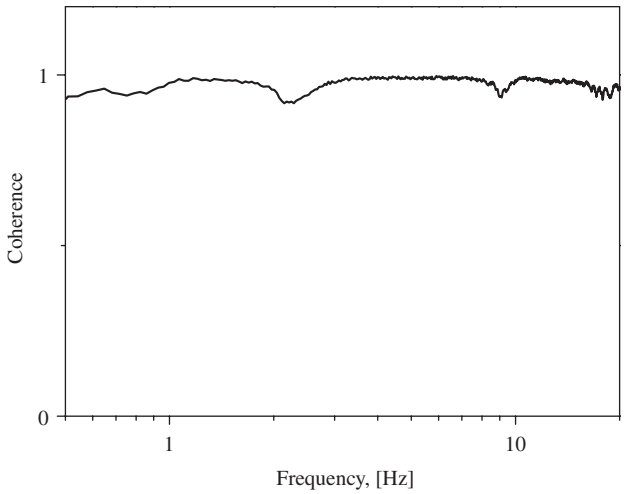

Fig. 18. Coherence between acceleration signals at the top (X_t)- and bottom (X_b)- of pneumatic vibration isolator; Hanning windowed, number of averages: 50, frequency resolution: 3.125×10^{-2} Hz.

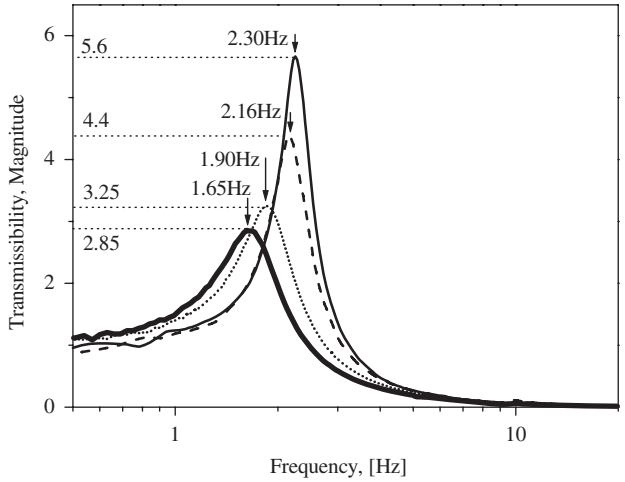

Fig. 19. Results of transmissibility measurements for increased total chamber volume and decreased stiffness of diaphragm without capillary tube; Hanning windowed, number of averages: 50, frequency resolution: 3.125×10^{-2} Hz (prototype(reference): ——, 3.6 times increase of total chamber volume:- - -, decreased stiffness of diaphragm by 50 percent: ....., increased total chamber volume as well as decreased stiffness of diaphragm: ——).

4.2. Experimental result

Fig. 19 represents a set of measured transmissibilities for various configurations of pneumatic vibration isolator without the capillary tube. Thin solid line shows the result of prototype(reference) with design specifications in Table 1. Although it should resemble a response of undamped single degree of freedom vibration isolation system since damping of capillary tube was eliminated, damping of diaphragm seems to cause a finite peak transmissibility 5.6 at resonance frequency 2.3 Hz. Two illustrations of proposed design method will be attempted for this prototype. One is to show the negative role of diaphragm stiffness. The other is to show an example of optimum transmissibility for a specific volume ratio N. It needs to be reminded that both the supplied pressure p_0 and the equivalent piston area A_p have been already determined by the condition of static-equilibrium with payload mass.

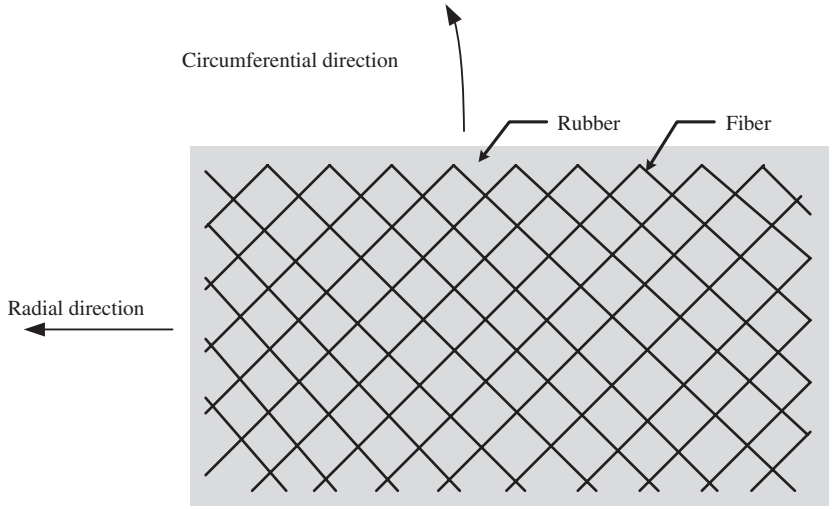

Fig. 20. Structure of diaphragm: fiber-reinforced rubber membrane (top-view).

Dotted line in Fig. 19 shows the measurement with decreased stiffness of diaphragm. By reducing the fiber density of diaphragm shown in Fig. 20, the stiffness of diaphragm could be decreased by approximately 50 percent of the current. This let the resonance frequency be decreased from 2.3 to 1.9 Hz by 0.4 Hz, and the peak transmissibility from 5.6 to 3.25 by 42 percent. This result was compared to transmissibility measurement represented with dash-line in Fig. 19, which was obtained after increasing the total chamber volume by 3.6 times of the prototype's one. The resonance frequency for this case reduces to 2.16 Hz from 2.3 Hz due to the decreased stiffness of air, but this is not satisfactory than the case of decreasing diaphragm stiffness. When the diaphragm with soft stiffness was applied to the configuration of increased chamber volume, the resonance frequency could be reduced from 1.9 to 1.65 Hz by 0.25 Hz as thick solid line shown in Fig. 19. That is, the effect of increasing chamber volume, i.e. decrement of resonance frequency is enlarged by replacing with a soft diaphragm. But it was only by 0.14 Hz before the replacement. From the above results, one can see the negative role of diaphragm stiffness in decreasing the resonance frequency of dual-chamber pneumatic vibration isolator. Thus, stiffness of diaphragm needs to be decreased as much as possible for preventing the negative effect of diaphragm. Efforts such as shape design of diaphragm by using FE code, which is highly recommended for future woks, can further decrease the diaphragm stiffness.

Next step for the isolator having both an increased chamber volume and a soft diaphragm as well is to show an example of optimum transmissibility. Since the optimum transmissibility varies with N, it is definitely right to determine the volume ratio N with the consideration of criteria for isolation performance. But, an example of optimum transmissibility for a specific N will be experimentally illustrated in this paper. To this end, the increased total chamber volume was divided in such way N has the value of '5'. In this case, the $C_{eq,op}(X_p)$ can be easily found to be $10.2 \times 10^5\,\mathrm{m}^{-1}$ with Eq. (19). Besides the dynamic amplitude X_p was estimated as 50 μm from the measurement of base acceleration. If we refer to Eq. (10), infinite combinations of the capillary tube geometry (L_c, D_c) satisfying the $C_{eq,op}(\bar{X}_p)$ would be possible. In this study, the values of L_c and D_c were determined as 8 and 0.77 mm, respectively, by considering the manufacturing limitation of capillary tube. Measurement result by newly designed capillary tube is shown with solid line in Fig. 21. For an identification weather it exhibits optimum transmissibility or not, two extreme cases of excluding- and blocking- the capillary tube were also measured and represented with dotted- and dashed-lines, respectively, in Fig. 21. It can be verified that three measurements nearly intersect at the frequency point 1.75 Hz, and that transmissibility by optimally designed capillary tube shows an almost zero slope at the frequency of intersection, i.e. minimization of peak transmissibility. Therefore, based on the above illustrations, the proposed method for optimum transmissibility design of pneumatic vibration isolator can be considered as very valid.

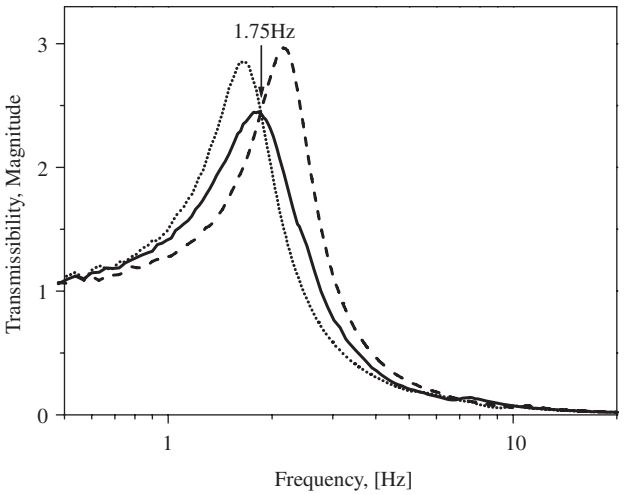

Fig. 21. Realization of optimum transmissibility; Hanning windowed, number of averages: 50, frequency resolution: 3.125×10^{-2} Hz (without capillary tube: ....., optimally designed capillary tube: ——, capillary tube blocked: - - -).

5. Concluding remarks

So far we have discussed a transmissibility design method for a dual-chamber pneumatic vibration isolator wherein a complex stiffness model developed in our previous research is adopted. A basic strategy for optimum design was established by making the frequency of the maximum loss factor coincide with the resonance frequency of transmissibility. An equivalent flow restriction coefficient $C_{eq}(X_p)$, obtained by approximating $C(X_p,\omega)$ to $\omega C_{eq}(X_p)$, was hereby proposed to derive the optimum damping tuning condition $C_{eq,op}(\bar{X}_p)$, which determines the optimum relation between $C_{eq}(\bar{X}_p)$ and the chamber volume ratio N for minimization of the peak transmissibility. Then, by varying N under the given total chamber volume, we could observe the trade-off among the resonance frequency of the optimum transmissibility, the peak value of transmissibility, and the transmissibility in the high frequency range. For the method of transmissibility design it was therefore suggested that N be pre-determined from negotiation of the required isolation performance, followed by design of the optimum transmissibility using $C_{eq,op}(\bar{X}_p)$ in Eq. (19). It is also critical to decrease the diaphragm stiffness in order to reduce the resonance frequency of optimum transmissibility.

Finally, it is considered that the proposed method of transmissibility design, validated from an experimental illustration, can be efficiently employed for the design of a dual-chamber pneumatic vibration isolator.

Acknowledgments

This work has been financially supported by the Center for Nanoscale Mechatronics and Manufacturing of KIMM (Korea Institute of Machinery and Materials) and R01-2006-000-10872-0 from the Basic Research Program of the KOSEF (Korea Science and Engineering Foundation). We also acknowledge Dr. Jun-Hwa Lee for commenting about treating amplitude-dependent isolation components in mechanical system.

Appendix A. Air flow modeling in the capillary tube

Fig. A1 shows typical velocity profiles in a circular capillary tube for the case of a steady flow [8]. At the entrance, the air flow cannot be smooth due to sharp corner, resulting in a rapid pressure drop known as Vena-contracta effect. As the air flows further into the capillary tube, viscosity of the air along the tube wall starts to govern the velocity profile, making parabolic at the end of entrance region. This is so called a fully developed flow, where the pressure is lost by the friction between air and the wall of the capillary tube. When the air reaches the exit, the velocity decreases once again causing an additional pressure loss. The total

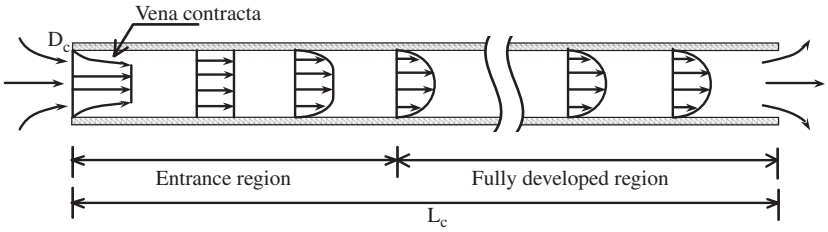

Fig. A1. Typical velocity profiles of steady air flow in capillary tube.

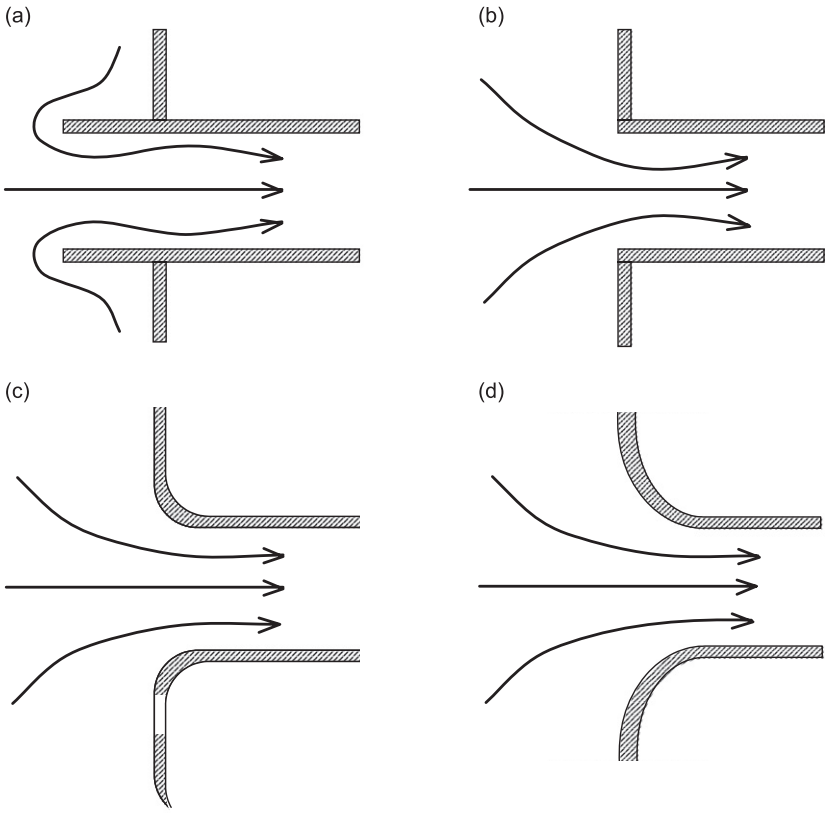

Fig. A2. Values of minor loss coefficient K according to inlet shape of capillary tube: (a) reentrant, $K = 0.8$, (b) sharp edge, $K = 0.5$, (c) rounded, $K = 0.2$ and (d) well rounded, $K = 0.04$.

pressure difference across the capillary tube Δp for dynamic flow can be expressed by the following equation:

$$\Delta p = \left(\frac{L_c}{D_c} fr(X_p, \omega) + K\right) \frac{4\rho}{3\pi} \left(\frac{A_p X_p \omega}{A_c}\right) u \tag{A.1}$$

which was quoted from Ref. [6] for convenience, where L_c and $D_c(A_c)$ denotes, respectively, the length and diameter(cross-sectional area) of the circular capillary tube, ρ the density of air, A_p the piston area, X_p and ω the input dynamic amplitude- and frequency- at the piston, respectively, u the velocity of lumped fluid element, and finally fr and K the coefficients for frictional- and minor-pressure loss, respectively. The friction coefficient fr, which will be explained in more detail later, varies from 0.01 to 1 with the fluid velocity u depending on whether the dynamic flow is unidirectional or oscillating. The minor loss coefficient K varies with location and

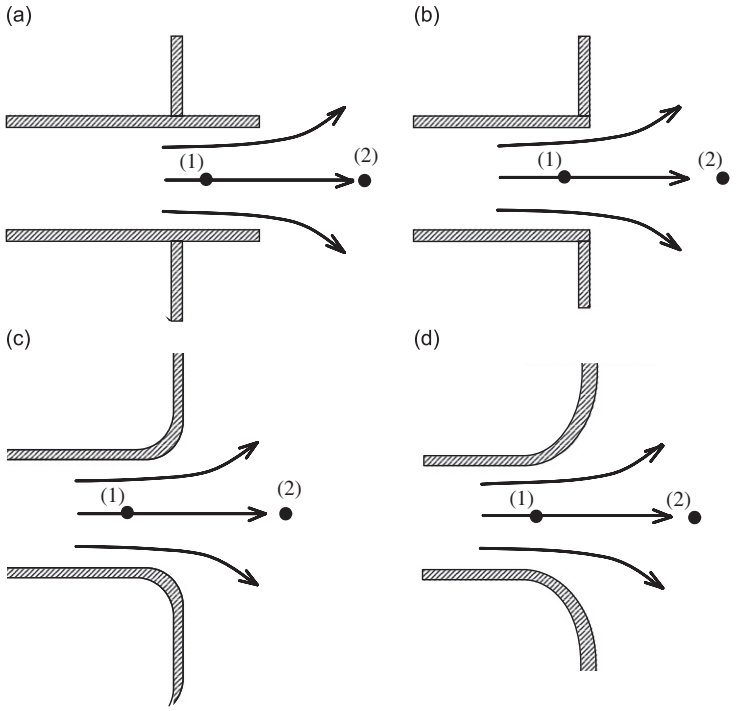

Fig. A3. Values of minor loss coefficient K according to outlet shape of capillary tube (a) reentrant, $K = 1.0$, (b) sharp edge, $K = 1.0$, (c) rounded, $K = 1.0$ and (d) well rounded, $K = 1.0$. *Note*: At the outlet of capillary tube, the entire kinetic energy of the existing fluid is dissipated as the stream of fluid mixes with the fluid in chamber and eventually comes to zero. The pressure loss from points (1)–(2) is therefore, $\Delta p = \rho(V_1^2 - V_2^2)/2 = \rho V_1^2/2 (= K\rho V_1^2/2)$. Thus the K value at the outlet of capillary tube does not vary with the outlet shape, but equals to one.

shape of capillary tube as shown in Figs. A2 and A3 [7]. Since shape of the capillary tube employed in this research is close to Figs. A2(b) and A3(a), K was accordingly taken as sum of 0.5 and 1.0, i.e. 1.5.

One can see from Eq. (A.1) that the total pressure difference across the capillary tube is composed of the frictional pressure loss in the tube wall and the minor pressure loss at the inlet- and outlet- of capillary tube. That is, the term $(L_c/D_c)fr$ in Eq. (A.1) represents the frictional pressure loss within the capillary tube, and K the dramatic pressure loss at the inlet- and outlet- of capillary tube. Contribution of minor pressure loss to the total pressure loss, often ignored in pipe flow problems where the pipe length would be far greater than its diameter, increases as the length-to-diameter ratio of capillary tube decreases and/or fluid velocity increases [7,8]. By taking the mean values of fr and K, we can infer that the frictional pressure loss can be significant compared with the minor one only provided that the length-to-diameter ratio is greater than 100. However, the length-to-diameter ratio of real capillary tubes typically ranges from 5 to 40, and, hence, the ratio of minor- to frictional-loss, i.e. $K/[(L_c/D_c)fr]$ was found to be about 0.3–5 in the frequency range of 2–5 Hz, where the damping of the capillary tube becomes very influential in pneumatic spring. These values increase with the increase of vibration amplitudes. The quantitative analysis so far shows the importance of not only the frictional pressure loss but also the minor one. Even though the additional pressure loss at the inlet- and outlet- of capillary tube is termed as the minor loss in the classical fluid dynamic theory, its contribution to the total pressure loss in this study is no more minor at all. Therefore the air flow in the capillary tube in dual-chamber pneumatic spring definitely needs careful consideration of the minor pressure loss as well as the frictional one, which was missed in Ref. [6].

The second issue concerning the friction coefficient fr is now to be discussed. As mentioned earlier, the friction coefficient takes different form according to the assumption of air flow, i.e. oscillating- or unidirectional-flow. Due to the reciprocating movement of piston, one may presume easily the governing air

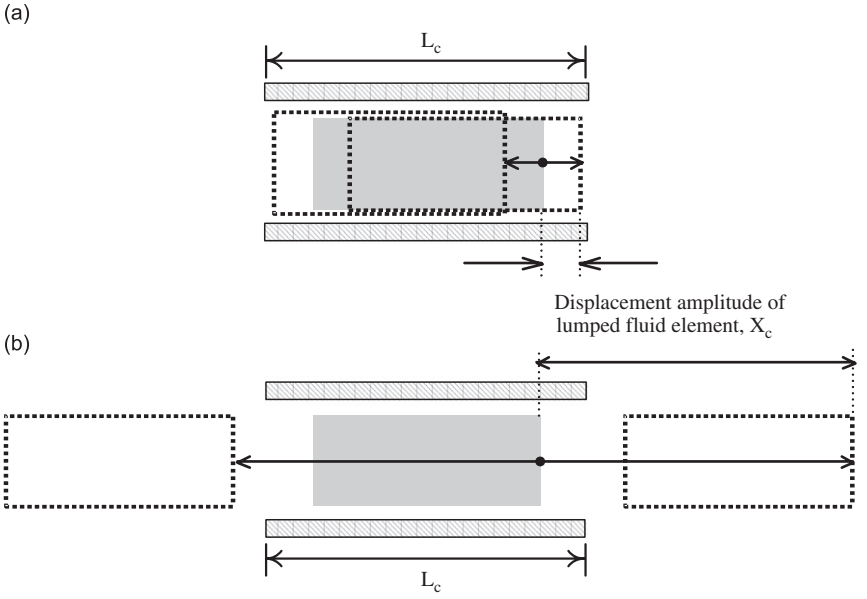

Fig. A4. Distinction between oscillating flow and unidirectional flow: (a) oscillating flow ($X_c < L_c$) and (b) unidirectional flow ($X_c < L_c$).

flow as oscillating one, as we have done in Ref. [6]. But the relation between amplitude of fluid displacement and length of capillary tube should be examined beforehand. As represented in Fig. A4(a), if the displacement amplitude of lumped fluid element X_c does not exceed the capillary length L_c, then the assumption of oscillating flow would be desirable. Otherwise, as shown in Fig. A4(b), the flow must be regarded as unidirectional one. It is easily calculated with the following continuity relation between the piston and capillary tube that the amplitude of fluid displacement X_c ranges several tens of centimeters corresponding to the case of Fig. A4(b).

$$A_c u_{max} = A_p \omega X_p \quad (u_{max} = \omega X_c) \tag{A.2}$$

This means that the flow characteristic in capillary tube is quite close to the unidirectional flow, not oscillating one. Hence it is more desirable to describe the frictional pressure loss with the unidirectional friction coefficient.

References

[1] C.G. Gordon, Generic criteria for vibration-sensitive equipment, *Proceedings of SPIE*, San Jose, CA, 1991.
[2] H. Amick, M. Gendreau, C.G. Gordon, Facility Vibration Issues for Nanotechnology Research, *Proceedings of the Symposium on Nano Device Technology*, Hsinchu, Taiwan, 2002.
[3] C.M. Harris, C.E. Crede, *Shock and Vibration Handbook*, McGraw-Hill, New York, 1961.
[4] D.B. DeBra, Design of laminar flow restrictors for damping pneumatic vibration isolators, *CIRP Annals* 33 (1) (1984) 351–356.
[5] C. Erin, B. Wilsonm, J. Zapfe, An improved model of a pneumatic vibration isolator: theory and experiment, *Journal of Sound and Vibration* 218 (1) (1998) 81–101.
[6] J.H. Lee, K.J. Kim, Modeling of nonlinear complex stiffness of dual-chamber pneumatic spring for precision vibration isolations, *Journal of Sound and Vibration* 301 (2007) 909–926.
[7] B.R. Munson, D.F. Young, T.H. Okiishi, *Fundamentals of Fluid Mechanics*, third ed., Wiley, New York, 1998.
[8] F.M. White, *Fluid Mechanics*, fifth ed., McGraw-Hill, New York, 2003.
[9] T.S. Zhao, P. Cheng, The friction coefficient of a fully-developed laminar reciprocating flow in a circular Pipe, *International Journal of Heat and Fluid Flow* 17 (2) (1996) 167–172.
[10] T.S. Zhao, P. Cheng, Experimental studies on the onset of turbulence and frictional losses in an oscillatory turbulent pipe flow, *International Journal of Heat and Fluid Flow* 17 (4) (1996) 356–362.
[11] J.S. Arora, *Introduction to Optimum Design*, second ed., Elsevier Academic press, 2004.
[12] S.H. Crandall, The role of damping in vibration theory, *Journal of Sound and Vibration* 11 (1) (1970) 3–18.

[13] A.S. Wineman, K.R. Rajagopal, *Mechanical Response of Polymers*, Cambridge University Press, Cambridge, 2000.
[14] N.W. Tschoegl, *The Phenomenological Theory of Linear Viscoelastic Behavior*, Springer, Berlin, 1989.
[15] J.H. Lee, R. Singh, Nonlinear frequency responses of quarter vehicle models with amplitude-sensitive engine mounts, *Journal of Sound and Vibration* 313 (2008) 784–805.
[16] T. Jeong, R. Singh, Inclusion of measured frequency and amplitude dependent mount properties in vehicle or machinery models, *Journal of Sound and Vibration* 245 (3) (2001) 385–415.
[17] J.P. Den Hartog, *Mechanical Vibrations (Section 3.3. The damped vibration absorber)*, fourth ed., Dover, New York, 1985.
[18] W.T. Thomson, M.D. Dahleh, *Theory of Vibration with Applications (Section 5.8. Vibration damper)*, fifth ed., McGraw-Hill, Prentice-Hall Inc., New York, 1998.
[19] J.H. Lee, K.J. Kim, Computation of complex dynamic stiffness of inflated diaphragm in pneumatic springs by using FE codes, *Proceedings of 13th International Conference on Sound and Vibration*, Vienna, Austria, 2006.
[20] J.S. Bendat, A.G. Piersol, *Random Data*, third ed., Wiley, New York, 2000.